

STRUCTURAL AND FTIR STUDIES OF PURE AND ZINC DOPED SnO_2 NANOPARTICLES

A. Amutha

The Standard Fireworks Rajaratnam College for Women, Sivakasi, India

ABSTRACT

Pure and zinc-doped tin oxide nanoparticles were synthesized by the chemical co-precipitation method. The structural studies were carried out by X-Ray Diffraction pattern. XRD pattern reveals the tetragonal rutile structure of tin oxide nanoparticles. Fourier Transform Infrared Spectroscopy studies were used to identify the chemical information of pure and zinc-doped tin oxide nanoparticles. The crystallite size of pure tin oxide nanoparticles is 9 nm obtained from the X-ray diffraction pattern. The Zn ions are incorporated into the tin ions. It is suitable candidate for gas sensor applications.

KEYWORDS

Tin oxide, semiconductor, nano particles, chemical method

1. INTRODUCTION

Introducing dopants into the nanoparticles may tune the microstructure which in turn, may enhance the gas sensing properties [1]. SnO_2 is a wide band gap (3.6 eV at room temperature) semiconductor. Zn doped SnO_2 nanostructures are enhancing the gas sensor response [2] [3] [4]. The ionic radius of Zn^{2+} is 0.073 nm which has the close value of Sn^{4+} ions (0.071 nm), so that Zn^{2+} can be incorporated into the SnO_2 lattice easily by substituting Sn^{4+} . The substitution of Zn^{2+} ions in the place of Sn^{4+} would result in a surface modification and formation of more oxygen vacancies which can enhance the gas sensing properties [2]. Decreasing the response time was observed with increasing the Zinc concentration in SnO_2 thin film [5]. Also, zinc doping can control the size of the SnO_2 nanorods which has significant applications in gas sensors. Mostly the pure and noble metal Pd, Pt doped SnO_2 nanostructures are reported [6] [7] [8]. The dopant corresponding to the SnO_2 nanostructure can be enhancing the gas sensing performance which is available in few reports. In this paper Zn doped SnO_2 is used to enhance the properties. The ionic radius of zinc is close to the ionic radius of Sn. Therefore, the Zn is substituted the Sn lattice site which could be created the lot of oxygen vacancy. The unit cell volume is decreased due to the doping of zinc in SnO_2 , therefore the size of nanostructure was decreased. In this work, Zn^{2+} doped SnO_2 nanoparticles were prepared by co-precipitation method. The FTIR studies were carried out. The influence of structural properties was studied by Zn doped SnO_2 nanoparticles.

2. EXPERIMENTAL PROCEDURE

Pure and Zn doped SnO_2 nanoparticles were prepared by chemical co-precipitation method. Tin Chloride ($\text{SnCl}_2 \cdot 2\text{H}_2\text{O}$) was used as precursor. Distilled water is used as solvent. Freshly prepared ammonia solution was added to the SnCl_2 solution. Then the solution was stirred to get precipitate. Finally, white precipitate was formed. The obtained nanoparticles were washed with doubly ionized water for several times. Then, the collected precipitate was heated at 100°C in a hot air oven to remove the water molecules. $\text{SnCl}_2 \cdot 2\text{H}_2\text{O}$ (0.05M) and ZnCl_2 (0.05M) was

dissolved in 100 ml of distilled water. Ammonia solution was added slowly to the precursor solution during stirring. This solution was stirring continuously still to get precipitate. Finally, the precipitate was centrifuged and dried at 100°C using hot air oven for 12 hours. This sample is taken as sample A. Further, varied the precursor concentration such as SnCl₂·2H₂O (0.06M) and ZnCl₂ (0.04M) denoted as sample B.

3. CHARACTERIZATION TECHNIQUES

3.1. FTIR (Fourier Transform Infrared Spectroscopy)

FTIR has been used to study the interaction between cations, anions and solvents. This interaction is determined by the shift in the IR spectrum as well as the alternation in the band shapes and intensities of internal vibration modes. Figure 1 represents the FTIR spectrum of pure tin oxide nano particles.

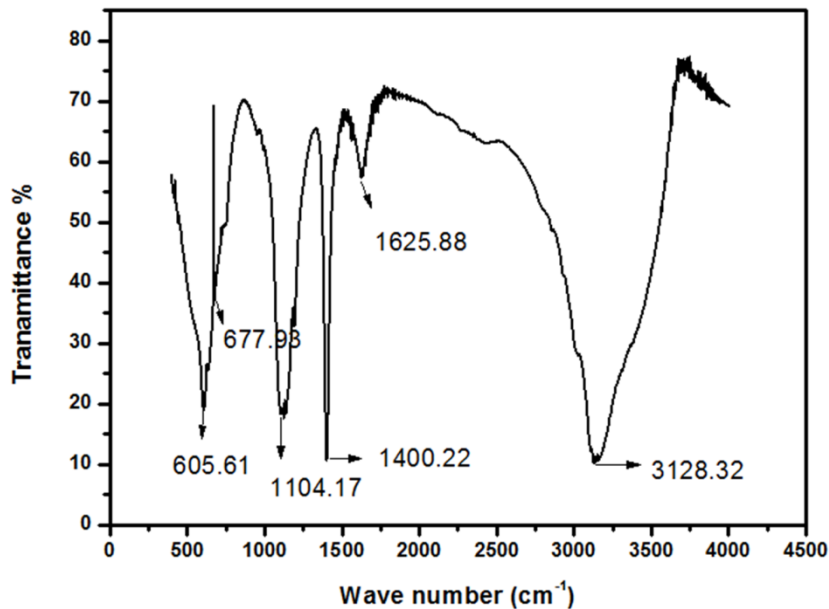


Figure 1. shows the FTIR spectrum of tin oxide nanoparticles.

Figure. 1 shows the FTIR spectrum of tin oxide nanoparticles. The band at 3128.32 cm⁻¹ is attributed due to O-H bonding. The band at 1625.88 cm⁻¹ is ascribed due to N-H bending. The band at 1400.22 cm⁻¹ is attributed to C=C stretching. The band at 1104.17 cm⁻¹ is ascribed due to O-H bending vibration. The bond at 677.93 cm⁻¹ and 605.61 cm⁻¹ are attributed due to Sn-O stretching vibration [9].

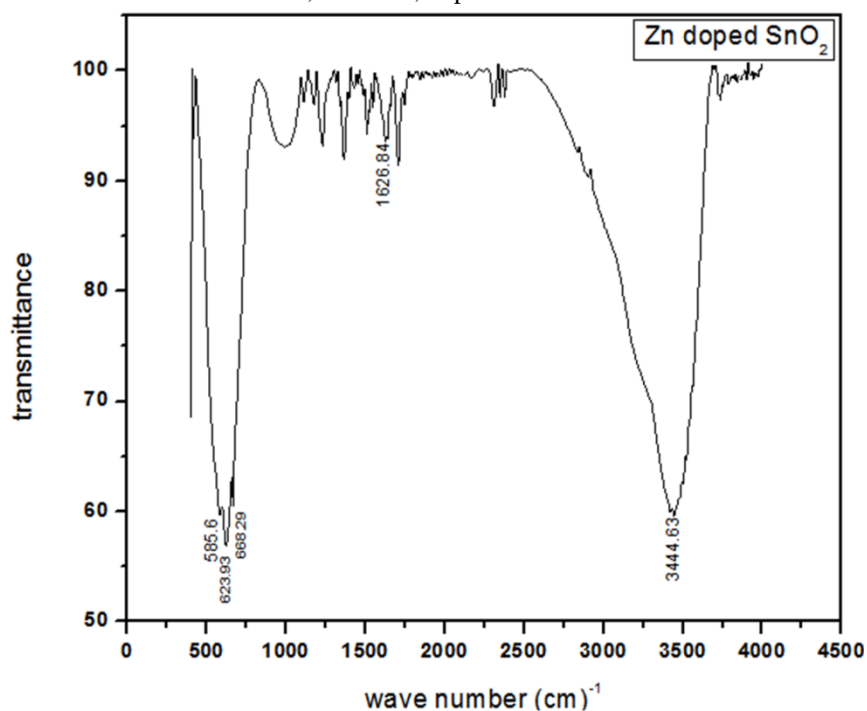


Figure 2. FTIR spectrum of Zn doped SnO₂ nanoparticle-Sample A.

Figure 2 shows the FTIR transmittance spectrum of the Zn doped tin oxide nanoparticles (Sample A). The absorption band 585.5 cm⁻¹ and 623.93 cm⁻¹ are ascribed due to the Sn-O stretching. The peak at 1113.81cm⁻¹ is related to the vibration of hydroxyl tin (Sn-OH) bond. The band at 1626.84 and 3444.63 cm⁻¹ is attributed due to the bending of strong broad O-H bonds.

TABLE 1. FTIR spectra of pure and Zn doped tin oxide nanoparticles (Sample A).

Observed Characteristics Frequency (cm) ⁻¹	Mode of Assignment
585.5 and 623.93	Sn-O stretching vibration
1113.81	Vibration of hydroxyl tin bond
1626 and 3444.63	Bending of OH bonds

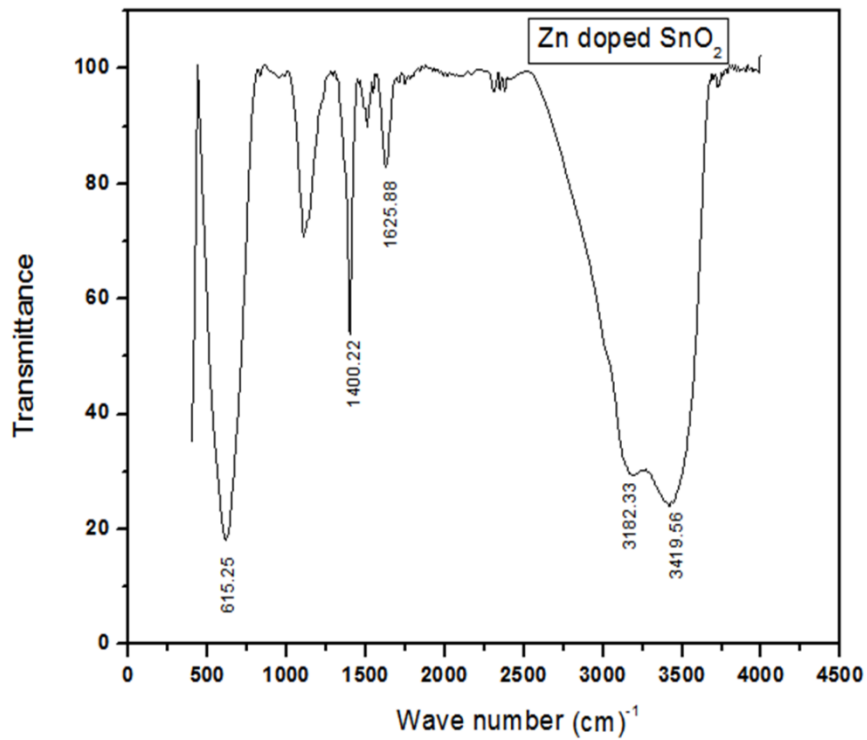


Figure 3. FTIR spectra of Zn doped SnO₂ nanoparticles-Sample B.

Figure 3. shows FTIR transmittance spectrum of the Zn doped tin nanoparticles (Sample B). The absorption bands at 615 cm⁻¹ is attributed due to anti-symmetric stretches of O-Sn-O. The peak at 1625 cm⁻¹ is appeared due to vibration of hydroxyl group. The wave numbers 3182 and 3419 cm⁻¹ are ascribed due to strong broad O-H stretching.

TABLE-2. FTIR spectra of pure and Zn doped tin oxide nanoparticles (Sample B)

Observed characteristics frequency (cm) ⁻¹	Mode of assignment
615	Anti symmetric stretches of O-Sn-O
1625	Hydroxyl group
3182 and 3419.5	Strong broad O-H stretching

3.2. X-RAY Diffraction Analysis

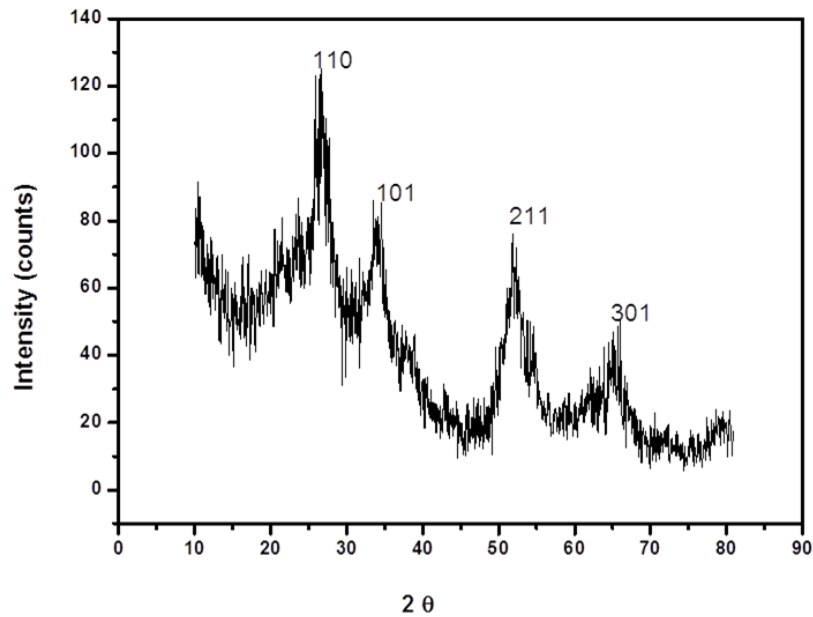


Fig. 4. XRD pattern of as prepared tin oxide nanoparticles

Figure 4 shows the XRD pattern which are indexed to (110), (101), (211) and (301) planes and it's confirmed the tetragonal structure of tin oxide.

The average particle size (D) was determined using the Scherer's equation.

$$D = K\lambda/\beta \cos\theta$$

Where D is the crystallite size, K is the shape factor, being equal to 0.9, λ is the X-ray wavelength, β is the full width at half maximum of the diffraction peak, and θ is the Bragg diffraction angle in degree. The average particles size was found to be 9 nm.

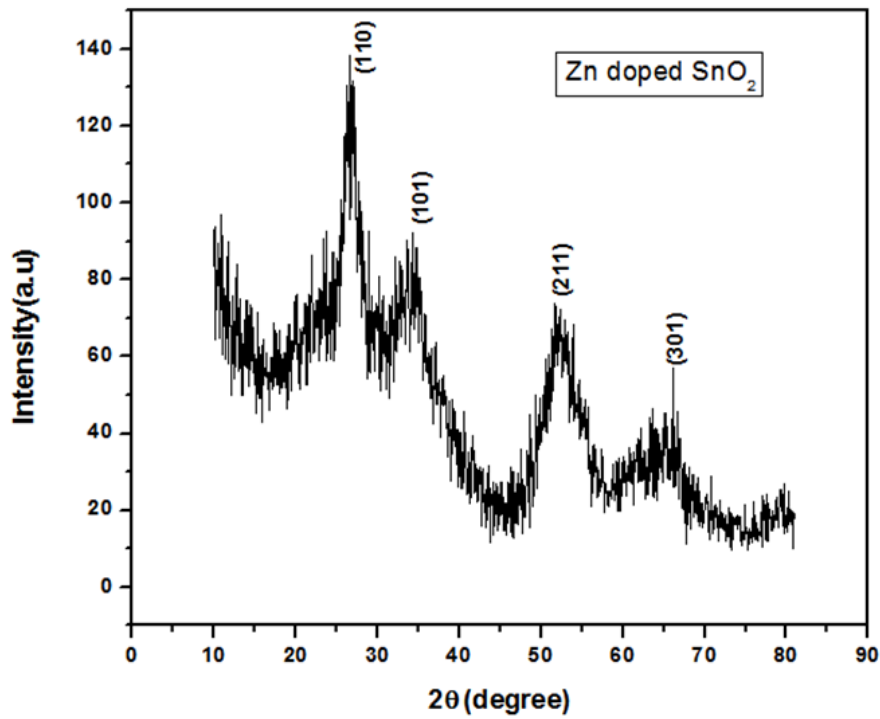


Figure-5. XRD pattern of SnO₂ nanoparticles-Sample A.

Figure 5 shows the XRD patterns of the Zn doped SnO₂ nanoparticles (Sample A). The XRD patterns are indexed to (110), (101) and (211) planes which reveals the tetragonal structure of SnO₂ (JCPDS card no 41-1445). The crystallite size was obtained from Debye Scherrer formula, $D = \frac{0.9\lambda}{\beta \cos\theta}$. The obtained crystalline size is 11 nm.

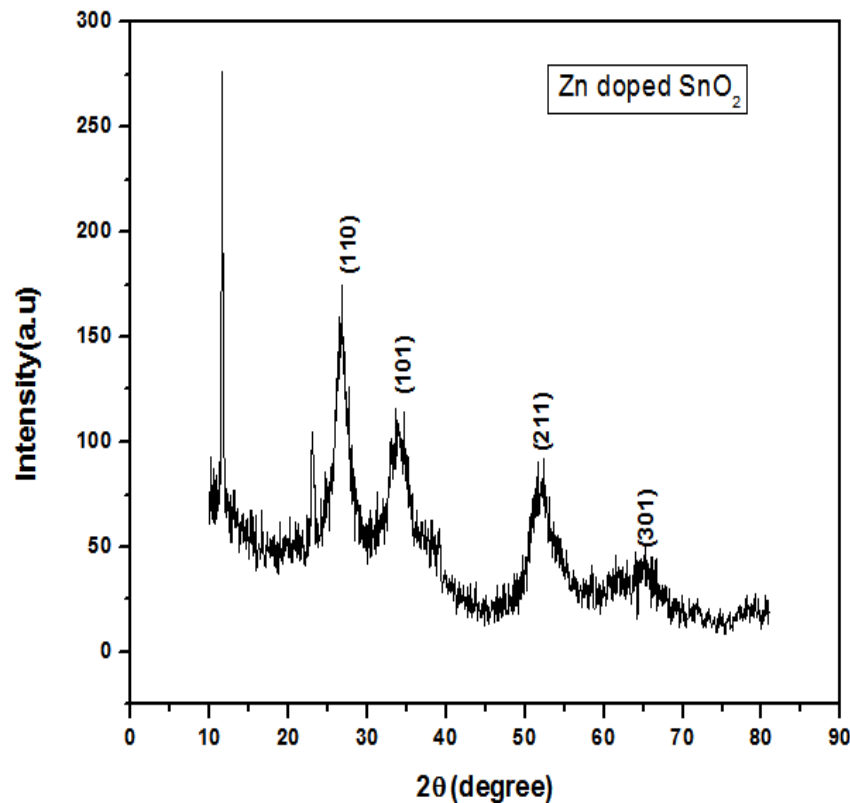


Fig 6. XRD pattern of Zn doped SnO₂ nanoparticles- Sample B

Figure 6 shows the XRD pattern of Zn doped tin oxide nanoparticles (Sample B). The XRD pattern is indexed to (110), (101) and (211) planes which reveals the tetragonal structure of SnO₂. The sharp peaks are observed when compared to pure SnO₂ and Sample A due to increasing the crystallinity of the sample. The average crystallites size is 15 nm estimated using the Scherrer's equation.

The FTIR and XRD patterns are confirmed the tetragonal structure of tin oxide. The crystallinity of the samples was increased with increasing the concentration of Zn when compared to pure tin oxide nanoparticles.

4. CONCLUSIONS

The pure and Zn doped tin oxide nanoparticles were successfully prepared by simple co-precipitation method. The pure and Zn doped nanoparticles were characterized by XRD and FTIR analysis. The vibrational bonds of tin oxide nanoparticles were analyzed using FTIR studies. The XRD analysis confirmed the crystalline nature of Tin oxide (SnO₂) nanoparticles. The crystallite size of pure tin oxide nanoparticles is 9 nm. Therefore, the size of the nanoparticles is below 10 nm. Hence, the tin oxide quantum dots have large surface to volume ratio. Therefore, the tin oxide is potential candidate for gas sensor applications.

REFERENCES

- [1] Z. Yuan, Rui Li, F. Meng, J. Zhang, K. Zuo and E. Han, *Sensors* 2019, Vol. 19, pp1495.
- [2] Gurpreet Singh, Jasmeet Kaur & Ravi Chand Singh, *AIP Conference Proceedings* 1675, 030042 (2015).
- [3] Parul Gupta & S K Sharma, *Mater. Res. Express*, Vol 4, No. 6 (2017).
- [4] Peng Sun, Lu You, Yanfeng Sun, Nianke Chen, Xianbin Li, Hongbo Sun, Jian Ma & Geyu Lu, *CrystEngComm*, (2012), 14, pp1701-1708.
- [5] S Vijayalakshmi, S Venkataraj, M Subramanian & R Jayavel, *J. Phys. D: Appl. Phys.* 41 035505 (2008).
- [6] M. D'Arienzo, L. Armelao, A. Cacciamani, C. Maria Mari, S. Polizzi, R. Ruffo, R. Scotti, A. Testino, L. Wahba & F. Morazzoni, *Chem. Mater.* 20102213 pp4083-4089.
- [7] Chang Liu, Qin Kuang, Zhaoxiong Xie and Lansun Zheng, *CrystEngComm* (2015) Vol. 17, pp 6308-6313.
- [8] David Degler, Sabrina A. Müller, Dmitry E. Doronkin, Di Wang, Jan-Dierk Grunwaldt, Udo Weimar & Nicolae Barsan, *J. Mater. Chem. A*, (2018)6, pp 2034-2046.